American Mineralogist, Volume 95, pages 1708–1716, 2010

The thermal equation of state of $FeTiO_3$ ilmenite based on in situ X-ray diffraction at high pressures and temperatures

E.J. Tronche,[1,*] M. van Kan Parker,[1] J. de Vries,[1,2] Y. Wang,[3] T. Sanehira,[3] J. Li,[4] B. Chen,[5] L. Gao,[6] S. Klemme,[7] C.A. McCammon,[8] and W. van Westrenen[1]

[1]Faculty of Earth and Life Sciences, VU University Amsterdam, De Boelelaan 1085, 1081 HV Amsterdam, The Netherlands
[2]Faculty of Geosciences, Utrecht University, Budapestlaan 4, 3584 CD Utrecht, The Netherlands
[3]Center for Advanced Radiation Sources, University of Chicago, 5640 Ellis Avenue, Chicago, Illinois 60637, U.S.A.
[4]Department of Geological Sciences, University of Michigan, Ann Arbor, Michigan 48109, U.S.A.
[5]Division of Geological and Planetary Sciences, California Institute of Technology, Pasadena, California 91125, U.S.A.
[6]Department of Geology, University of Illinois Urbana-Champaign, 1301 West Green Street, Illinois 61801, U.S.A.
[7]Institut für Mineralogie, Corrensstrasse 24, D-48149 Münster, Germany
[8]Bayerisches Geoinstitut, Universität Bayreuth, D-95440 Bayreuth, Germany

Abstract

We present in situ measurements of the unit-cell volume of a natural terrestrial ilmenite (Jagersfontein mine, South Africa) and a synthetic reduced ilmenite ($FeTiO_3$) at simultaneous high pressure and high temperature up to 16 GPa and 1273 K. Unit-cell volumes were determined using energy-dispersive synchrotron X-ray diffraction in a multi-anvil press. Mössbauer analyses show that the synthetic sample contained insignificant amounts of Fe^{3+} both before and after the experiment. Results were fit to Birch-Murnaghan thermal equations of state, which reproduce the experimental data to within 0.5 and 0.7 GPa for the synthetic and natural samples, respectively. At ambient conditions, the unit-cell volume of the natural sample [$V_0 = 314.75 \pm 0.23$ (1σ) Å^3] is significantly smaller than that of the synthetic sample [$V_0 = 319.12 \pm 0.26$ Å^3]. The difference can be attributed to the presence of impurities and Fe^{3+} in the natural sample. The 1 bar isothermal bulk moduli K_{T0} for the reduced ilmenite is slightly larger than for the natural ilmenite (181 ± 7 and 165 ± 6 GPa, respectively), with pressure derivatives $K_0' = 3 \pm 1$. Our results, combined with literature data, suggest that the unit-cell volume of reduced ilmenite is significantly larger than that of oxidized ilmenite, whereas their thermoelastic parameters are similar. Our data provide more appropriate input parameters for thermo-chemical models of lunar interior evolution, in which reduced ilmenite plays a critical role.

Keywords: Ilmenite, equation of state, X-ray diffraction, lunar magma ocean

Introduction

Ilmenite (nominal composition $FeTiO_3$) plays a pivotal role in current models of the thermal and magmatic evolution of the Moon (e.g., Shearer et al. 2006; Klemme et al. 2006), although it is only found as an accessory phase in terrestrial crustal and upper mantle rocks. Its crystallization during the later stages of the solidification of a global lunar magma ocean resulted in a gravitationally unstable mineral stratification in the lunar mantle (e.g., Taylor 1982; Snyder et al. 1992), prompting a large-scale mantle overturn (e.g., Hess and Parmentier 1995; de Vries et al. 2010). The thermal effects associated with this overturn are believed to have triggered the formation and eruption of the lunar mare basalts that cover a significant part of the lunar near-side surface (e.g., Lucey et al. 2006).

Thermo-chemical models of the internal evolution of the Moon thus require accurate knowledge of the density of ilmenite as a function of pressure (P), temperature (T), and chemical composition. Due to its limited importance for the dynamics of the interior of the Earth, the thermal equation of state of $FeTiO_3$ ilmenite has not been studied extensively. As a result, the temperature dependence of the bulk modulus, and pressure dependence of thermal expansivity are poorly constrained. In addition, the reducing conditions on the Moon lead to the absence of Fe^{3+} in lunar ilmenite, whereas in terrestrial ilmenite 15–30% of iron is trivalent (e.g., Virgo et al. 1988). The effects of oxidation state on ilmenite's density evolution are not known.

In this paper, we compare the P-T variation of the unit-cell volume of a synthetic Fe^{3+}-free ilmenite with that of a natural terrestrial ilmenite at simultaneous high P-T, to determine the thermal equation of state of ilmenite and its dependence on the valence state of iron.

Previous work

Ilmenite ($FeTiO_3$) is an iron-titanium oxide crystallizing in the trigonal system (space group $R\bar{3}$). Its structure was first studied by Barth and Posnjak (1934) and was found to be equivalent to the corundum structure. Detailed crystal-structural data at ambient pressure-temperature conditions have since been reported for natural terrestrial ilmenite (Raymond and Wenk 1971; Bayer et al. 1972; Liu 1975; Thorpe et al. 1977; Ming et al. 2006), synthetic ilmenite (Shirane et al. 1962; Syono et al. 1981; Wechsler and Prewitt 1984), and lunar ilmenite (Raymond and Wenk 1971;

* E-mail: elodie.tronche@falw.vu.nl

Bayer et al. 1972; Thorpe et al. 1977).

Studies at elevated temperature or pressure were limited to Wechsler and Prewitt (1984), who measured the unit-cell volume evolution of synthetic ilmenite at high temperature and room pressure, and at high pressure and room temperature. Yamanaka et al. (2007) also assessed the behavior of $FeTiO_3$ at high pressure and room temperature. To date, no data are available at simultaneous high pressure and high temperature.

The unit-cell volumes at ambient pressure-temperature conditions, V_0, reported in these studies are summarized in Table 1. The V_0 of lunar ilmenite is ~0.15% larger than that of terrestrial samples, mainly due to an elongated *c* axis (Table 1). This observation has been explained by the difference in oxidation states of Fe and Ti caused by the more reduced conditions on the Moon (Bayer et al. 1972; Thorpe et al. 1977). It is, therefore, necessary to determine the effect of iron oxidation state on the density and elasticity of ilmenite. It should be noted that lunar ilmenite also contains different concentrations of minor elements such as Mg compared to terrestrial samples, which affect their unit-cell volume as well.

Experimental and analytical methods

Starting materials

A natural sample and a synthetic sample were investigated in this study. The natural sample was a large (6 mm in diameter) homogenous ilmenite clast from the Jagersfontein kimberlite mine, South Africa. Its measured major element composition (Table 2) falls within the range of South African on-craton kimberlite samples (Wyatt et al. 2004) although its chromium content is lower than average. The clast contains very few small (1 μm in diameter) Ti-rich inclusions along grain boundaries, which are volumetrically insignificant and have not been detected on X-ray diffraction patterns.

Synthetic Fe^{3+}-poor ilmenite was produced in the gas-mixing furnace at the Institut für Mineralogie in Münster (Germany) using general procedures described by Klemme et al. (2006). High-purity oxides (Fe_2O_3 99.99%, TiO_2 99.99%) in the appropriate molar proportions were mixed in an agate mortar under acetone. The powder was then pelletized, placed in a Pt-wire basket and inserted into a vertical gas-mixing furnace, which was heated to T = 1073 K under a gas mixture of CO/CO_2 ($\Delta\log f_{O_2} = -0.02$). Oxygen fugacity in the furnace was controlled by varying proportions of CO and CO_2 in the furnace with Tylan digital gas flow controllers. The temperature was slowly raised to 1373 K at a rate of 3 K/min. The sample was equilibrated at 1373 K and constant f_{O_2} for 21 h. Then the temperature of the furnace was lowered to 1173 K at a rate of 3 K/min and the gas mixture was adjusted to CO/CO_2 = 170/30. The sample was kept at these conditions for another 14 h, and then quenched in water. Post-synthesis X-ray diffraction and Raman spectroscopy analyses at the Institut für Mineralogie in Münster confirmed that the synthesized sample was pure ilmenite. Both starting materials were ground in ethanol to a very fine powder and stored under dry conditions until use.

Table 1. Compilation of literature lattice parameters (in angstroms) and corresponding unit-cell volumes (in cubic angstroms)

Source	Sample	*a*	*c*	V_0
Raymond and Wenk (1971)	Natural terrestrial	5.091	14.056	315.499
Bayer et al. (1972)	Natural terrestrial	5.092	14.026	314.95
Liu (1975)	Natural terrestrial	5.075	13.972	311.646
Thorpe et al. (1977)	Natural terrestrial	5.090	14.046	315.151
Ming et al. (2006)	Natural terrestrial	5.079	14.187	316.953
Ming et al. (2006)	Natural terrestrial	5.090	14.056	315.376
This study	Natural terrestrial	5.093	14.012	314.750
	Average natural terrestrial	5.087	14.052	314.933
Raymond and Wenk (1971)	Lunar (sample 10085)	5.085	14.088	315.4728
Bayer et al. (1972)	Lunar (sample 10047)	5.089	14.082	315.785
Thorpe et al. (1977)	Lunar (sample 10047)	5.081	14.08	314.798
	Average lunar	5.085	14.083	315.352
Shirane et al. (1962)	Synthetic	5.087	14.085	315.654
Syono et al. (1981)	Synthetic	5.087	14.084	315.569
Wechsler and Prewitt (1984)	Synthetic before heating	5.088	14.086	315.839
Wechsler and Prewitt (1984)	Synthetic after heating	5.089	14.093	316.076
Yamanaka et al. (2007)	Not reported	5.0881	14.091	315.9248
	Average synthetic	5.088	14.088	315.813
This study	Synthetic, reduced	5.11	14.11	319.12

P-V-T measurements

High-pressure, high-temperature experiments were performed in the 1000 ton multi-anvil press at beamline 13-ID-D of the Advanced Photon Source (APS, Argonne National Laboratory, Illinois, U.S.A.) (Wang et al. 2009). The high-pressure assembly, shown in Figure 1, was developed specifically for in situ experiments by the COnsortium for Materials Properties Research in Earth Sciences (COMPRES) (Leinenweber et al. 2006). It is based on an octahedron with 10 mm edge length, made of a mixture of $MgAl_2O_4$ spinel and MgO (Leinenweber, personal communication). A rhenium foil furnace of thickness 0.025 mm was wrapped within a $LaCrO_3$ insulating sleeve, inserted into the center of the octahedron. Two windows were cut through the $LaCrO_3$ and rhenium furnace and filled with graphite, to allow the synchrotron X-ray beam to pass through the assembly with little absorption. Pyrophyllite gaskets were used to separate the eight second-stage Toshiba F-grade tungsten carbide cubes with 5 mm truncated-edge lengths.

The starting material was packed between rhenium disks to minimize sample oxidation (van Westrenen et al. 2005). We used high-purity MgO (99.99 wt%, fired at 1273 K for 20 h) as a pressure calibrant, which was mixed with strongly absorbing platinum powder to help determining the calibrant location at high *P* and *T*.

Temperatures were measured with a W5%Re-W26%Re (type C) thermocouple inserted axially in the assembly. No account was taken of the effect of pressure on the thermocouple electromotive force (emf). Temperatures were controlled to within 5 K. The thermocouple hot junctions were located ~1 mm from the sample in all runs (Fig. 1), within the X-ray window of the assembly. Thermal mapping of similar high-pressure assemblies using spinel layer growth kinetics (van Westrenen et al. 2003) has shown that the temperature difference between thermocouple junction and sample is less than 20 K in this case.

Samples were initially pressurized at room temperature. Six experiments were performed using the natural starting material, seven using the synthetic ilmenite starting material, at nominal hydraulic ram load between 40 and 445 metric tons. At each nominal ram load, samples were heated to 1273 K at a rate of ~100 K/min. To minimize sample oxidation, higher temperatures were not applied. Samples were subsequently cooled down step-wise to room temperature, with synchrotron X-ray diffraction measurements collected at 100 to 200 K intervals. Pressure-temperature conditions for all X-ray diffraction measurements are shown in Figure 2. Approximately 15 min were spent at each temperature to collect diffraction patterns of the pressure calibrant and the sample. After quenching to room temperature, the sample was compressed further in preparation for the next set of measurements.

Table 2. Major and minor element composition (in wt%) of samples used in this study, both before (b.e.) and after (a.e.) high-pressure, high-temperature experiment

	SiO_2	TiO_2	Al_2O_3	Cr_2O_3	FeO	MnO	MgO	CaO	Total	*n*
Natural ilmenite (Jagersfontein mine, South Africa)										
b.e.	0.06(7)	48.41(10)	0.67(7)	0.02(1)	41.83(32)	0.19(1)	7.90(8)	0.02(1)	99.28(23)	10
a.e.	0.17(26)	48.93(50)	0.59(7)	0.00(0)	41.9(11)	0.18(2)	7.72(2)	0.03(2)	99.50(27)	10
Synthetic ilmenite										
b.e.	0.02(0)	53.56(10)	0.01(0)	n.a.	47.67(6)	0.00(0)	0.00(0)	0.01(0)	101.27(27)	15
a.e.	0.03(0)	52.73(40)	0.03(0)	n.a.	48.69(8)	0.00(0)	0.00(0)	0.01(0)	101.49(7)	15

Notes: n.a. = not analyzed

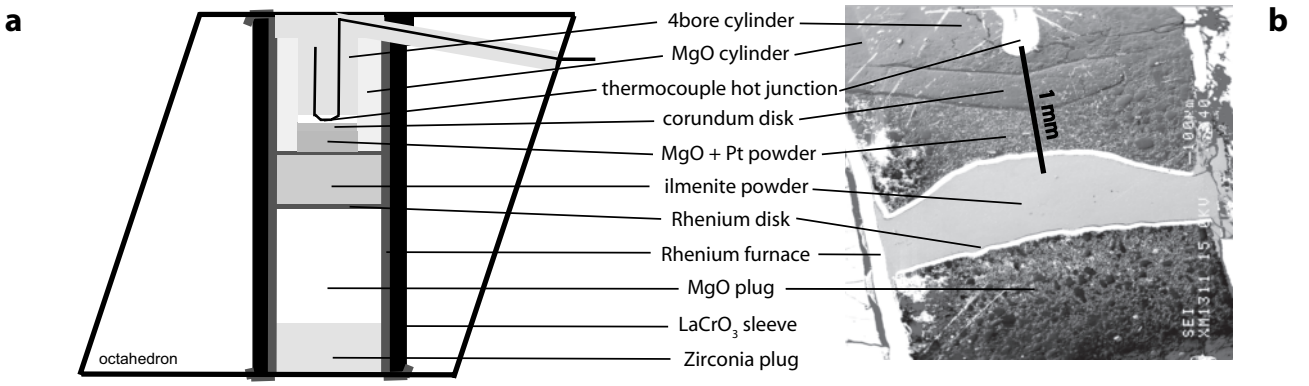

FIGURE 1. Experimental setup. (**a**) Sketch of the assembly. (**b**) Scanning electron microscope image of a section through a typical experimental charge. For details see text.

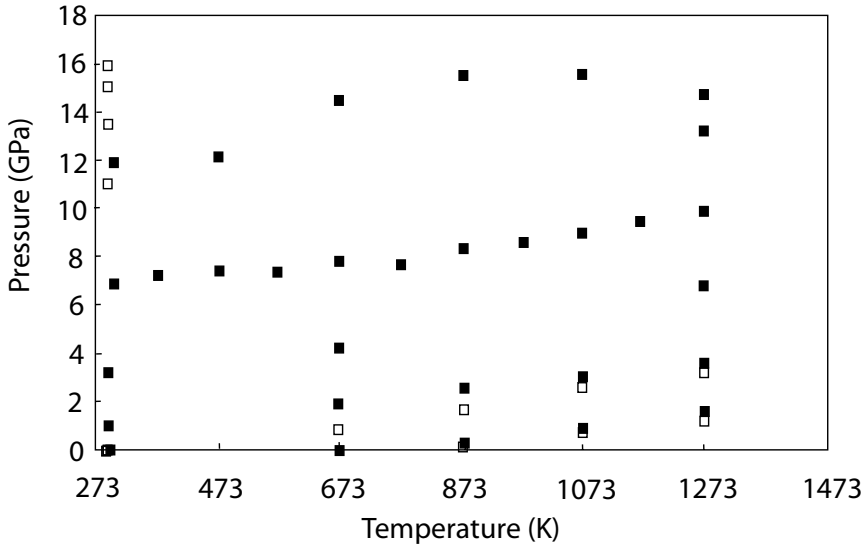

FIGURE 2. Pressure-temperature conditions applied in our experiments (solid squares = synthetic reduced ilmenite sample; open squares = natural terrestrial ilmenite sample).

Analytical methods

Energy-dispersive synchrotron X-ray diffraction patterns of MgO and ilmenite were obtained at each *P-T* point. Positions of the pressure calibrant and the sample were identified using radiograph images on a CoolSNAP CCD camera, with an imaging scintillator inserted into the beam path. The diffracted X-ray beam was then detected with a Canberra Ge solid-state detector placed at a 2θ angle of ~6°. Synchrotron X-ray diffraction patterns of MgO and the samples were analyzed using the Le Bail fitting technique in the software package GSAS (Larson and von Dreele 2004) with the EXPGUI program (Toby 2001). Between 3 and 5 peaks were used to refine the MgO unit cell, and 11 to 14 peaks to refine the *a* and *c* lattice parameters of the ilmenite unit cell. The detector 2θ angle was calibrated before pressurization by fitting four Pt or five MgO peaks. MgO unit-cell volumes were converted to pressures using the Speziale et al. (2001) thermal equation of state. At the *P-T* conditions of this study, this EOS gives results that are identical within error to those derived using the more recent MgO EOS of Tange et al. (2009).

Electron microprobe analyses of both starting materials and run products were performed using the JEOL JXA-8800M at VU University Amsterdam (Netherlands) to check for homogeneity and assess the extent of compositional changes during the experiments. An accelerating voltage of 15 kV and a beam current of 15 nA were applied, with a 5 µm diameter beam size. A synthetic ilmenite was used as the standard, and ZAF correction was applied.

Mössbauer analyses were performed on the synthetic ilmenite both before and after the experiments, to constrain its Fe^{3+} contents. The natural ilmenite used for this study has also been analyzed. Approximately 2 mg of the synthetic starting material was crushed in an agate mortar under ethanol and glued over a 4 mm diameter spot on a mylar sheet. Based on the ilmenite chemical composition (Table 2) and the sample weight and diameter, the effective Mössbauer thickness was estimated to be 6 mg Fe/cm^2. For Mössbauer analyses of the synthetic run product, the entire octahedral cell assembly was cut in half and polished to a thickness of 100 µm.

Mössbauer spectra were recorded at room temperature in transmission mode on a constant acceleration Mössbauer spectrometer with a nominal 1.85 GBq ^{57}Co source in a 6 µm Rh matrix for the starting material, and a nominal 370 MBq ^{57}Co high specific activity source in a 12 µm thick Rh matrix for the run product. The velocity scale was calibrated relative to a 25 µm thick α-Fe foil using the positions certified for (former) National Bureau of Standards standard reference material no. 1541; line widths of either 0.28 mm/s (starting material) or 0.36 mm/s (run product) for the outer lines of α-Fe were obtained. Spectra were fit using the commercially available fitting program NORMOS written by R.A. Brand (distributed by Wissenschaftliche Elektronik GmbH, Germany).

RESULTS

Sample compositions

It is important to ascertain that sample compositions did not change significantly during the in situ experiments. Potential problems in this particular study include ilmenite alteration by incorporation of magnesium from the MgO layers above and below the Re disks bounding the samples (Fig. 1) and ilmenite

oxidation by conversion from Fe^{2+} to Fe^{3+}. Electron microprobe and Mössbauer analyses of starting materials and run products show that the extent of these problems was insignificant.

Electron microprobe data for the starting materials and run products are summarized in Table 2. The major and minor element compositions of the natural sample are virtually identical before and after the experiments. Some small areas within 10 μm of the edge of the ilmenite sample chamber show slightly elevated magnesium contents (up to 0.3 wt% MgO), probably due to the fact that the Re disks did not fully isolate the sample from the rest of the assembly. However, all X-ray diffraction patterns were taken near the center of the charge, avoiding these slightly contaminated areas.

Mössbauer spectra of both samples are dominated by a slightly asymmetric quadrupole doublet, accompanied by a component with significantly smaller absorption (Fig. 3). This is consistent with the Mössbauer spectra of natural ilmenite reported previously in the literature (Virgo et al. 1988). The data were fitted to two quadrupole doublets with Lorentzian line shape corresponding to Fe^{2+} and Fe^{3+}, using conventional constraints (i.e., equal component widths and areas). Estimated standard deviations were derived from the statistics of the fitting process as well as uncertainties in the fitting model itself. $Fe^{3+}/\Sigma Fe$ were estimated from the relative areas to be 6 ± 2% (1σ) for the starting material of the synthetic ilmenite and 3 ± 2% for the synthetic run product after experiments. These values are much smaller than those found in terrestrial, more oxidized ilmenites (15–30%, Virgo et al. 1988). In comparison, the natural ilmenite powder used for this study was found to contain $Fe^{3+}/\Sigma Fe$ of 28 ± 3%. The Mössbauer results are also consistent with mass balance calculations using the electron microprobe data, which show that the synthetic ilmenite contains a very small amount of Fe^{3+} (3.4% Fe_2O_3, 96.6% FeO). Together, these data confirm that the experimental assembly used does not lead to significant iron oxidation (van Westrenen et al. 2005). The limited increase in Fe^{3+} content in synthetic ilmenite compressed at room temperature reported by Wu et al. (2009) did not occur in our experiments.

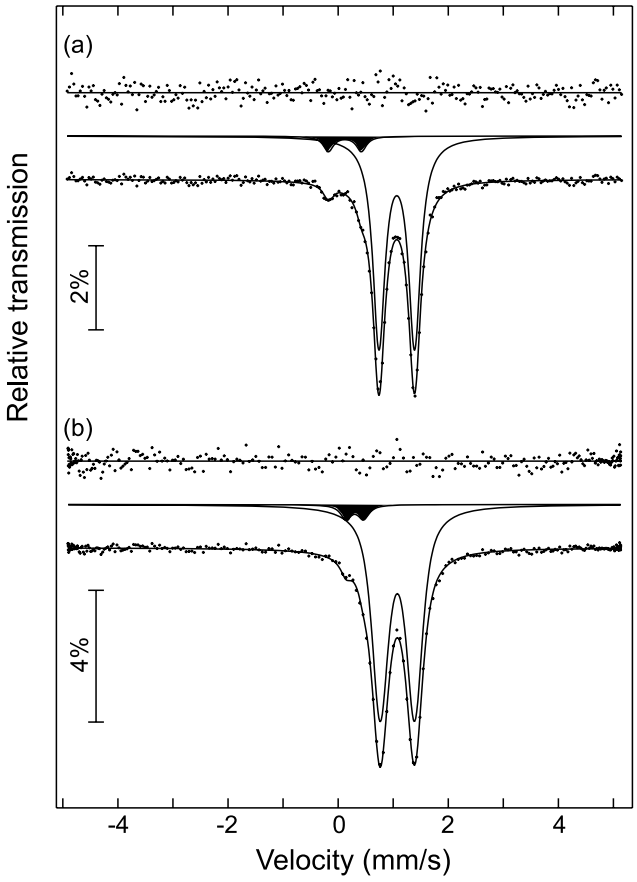

FIGURE 3. Mössbauer analysis results for a synthetic ilmenite before experiment (**a**) and after experiment (**b**).

Lattice parameters and equations of state

Tables 3 and 4 display the *P* values obtained from the refined MgO lattice parameters and the refined lattice parameters and resulting unit-cell volumes of the natural and synthetic ilmenite, respectively. For some measurements at the highest nominal pressures, Re disk interference prevented reliable extraction of unit-cell parameters for the calibrant and/or the sample. At the relatively low pressures involved, the relaxation of the experimental assembly at high temperature was such that sample pressures were close to ambient even at a nominal pressure of 41 metric tons.

None of our spectra showed evidence for the presence of the high-pressure perovskite phase of $FeTiO_3$. This is consistent with the position in *P-T* space of the ilmenite-perovskite phase boundary determined in situ by Ming et al. (2006) using the same APS beamline as employed in this study.

The *P-T* evolution of *a*, *c*, and *V* for both ilmenite samples is shown in Figure 4. As observed previously (e.g., Wechsler and Prewitt 1984) the structure compresses anisotropically, with the *c* axis being approximately twice as compressible as the *a* axis. Thermal expansion, on the other hand, is slightly more pronounced for the *a* axis than for the *c* axis.

Unit-cell volumes were fit to a third-order Birch-Murnaghan thermal equation of state (EOS), using the program EOSfit (Angel 2000). This thermal EOS relates the unit-cell volume *V* at pressure *P* and temperature *T* to the isothermal bulk modulus at 1 bar K_{T0} and its pressure derivative K_0', and the zero-pressure unit-cell volume $V_{0(T)}$ at temperature *T* (Eq. 1).

$$P(V,T) = \frac{3}{2}K_{T0}\left[\left(\frac{V_0(T)}{V}\right)^{7/3} - \left(\frac{V_0(T)}{V}\right)^{5/3}\right] \times \left\{1 + \frac{3}{4}\left(K_0' - 4\right)\left[\left(\frac{V_0(T)}{V}\right)^{2/3} - 1\right]\right\} \quad (1)$$

$V_{0(T)}$ is described in terms of the zero-pressure unit-cell volume at room temperature, V_0, and the thermal expansivity parameters α_0 and α_1 following Equation 2.

$$V_0(T) = V_0 \exp\left(\alpha_0\left(T - T_0\right) + \frac{1}{2}\alpha_1\left(T^2 - T_0^2\right)\right) \quad (2)$$

Fit results are given in Table 5, together with the previously published estimate of Wechsler and Prewitt (1984), which was not based on measurements at simultaneous high *P* and high *T*. The errors in the EOS parameters were propagated from the errors in the pressure determination and in the ilmenite

TABLE 3. Pressure, temperature, and unit-cell volume measurements for natural ilmenite (Jagersfontein Mine)

Nominal pressure (metric tons)	*T* (K)	*a* (MgO)	*P* (GPa)	*a* (Ilm)	*c* (Ilm)	*V* (Ilm)	Δ*P* (GPa)
41	1273	4.2611(2)	1.11(1)	5.1331(3)	14.1188(15)	322.438(33)	0.17
41	1073	4.2531(3)	0.61(1)	5.1239(3)	14.1000(14)	320.797(32)	–0.02
41	873	4.2461(2)	0.008(8)	5.1178(3)	14.0917(14)	320.024(33)	0.17
41	673	4.2357(3)	0	5.1087(3)	14.0659(15)	318.323(33)	0.25
41	298	4.2177(2)	0	5.0901(3)	14.0151(15)	314.956(33)	0.002
59	1273	4.2421(3)	3.10(1)	5.1141(3)	14.0402(14)	318.492(30)	0.03
59	1073	4.2357(2)	2.45(1)	5.1077(3)	14.0331(15)	317.746(32)	0.15
59	873	4.2315(2)	1.57(1)	5.1033(3)	14.0262(15)	316.887(32)	–0.06
59	673	4.2258(2)	0.88(1)	5.1004(4)	14.0102(18)	315.737(40)	–0.33
0	298	4.2190(2)	0	5.0901(2)	14.0100(15)	314.343(40)	–0.4
272	298	4.1340(2)	11.06(1)	5.0100(4)	13.5800(20)	295.193(100)	–0.72
318	298	4.1180(2)	13.47(1)	4.9900(4)	13.5500(20)	292.194(101)	–0.45
363	298	4.1080(2)	15.03(1)	4.9805(4)	13.5207(20)	290.380(98)	–0.22
408	298	4.102(2)	15.99(1)	4.9798(4)	13.5030(20)	289.950(98)	0.41

Note: Lattice parameters *a* and *c* for MgO and ilmenite given in angstroms, unit-cell volumes *V* given in cubic angstroms. Numbers in parentheses are 1σ error in last digit. Δ*P* denotes difference between measured *P* and *P* calculated for given *T* and ilmenite unit-cell volume *V* using the Birch-Murnaghan (BM) EOS parameters listed in Table 5.

TABLE 4. Pressure, temperature, and unit-cell volume measurements for synthetic ilmenite

Nominal pressure (metric tons)	*T* (K)	*a* (MgO)	*P* (GPa)	*a* (Ilm)	*c* (Ilm)	*V* (Ilm)	Δ*P* (GPa)
45	1273	4.2574(3)	1.42(2)	5.1438(4)	14.164(2)	324.552(41)	0.29
45	1075	4.2532(4)	0.74(2)	5.132(0)	14.160(2)	322.976(44)	–0.22
45	874	4.2460(4)	0.28(2)	5.1283(4)	14.155(2)	322.383(39)	–0.09
45	673	4.2371(4)	0	5.1231(4)	14.160(2)	321.604(39)	0.03
45	290	4.2184(3)	0	5.1116(4)	14.125(2)	319.633(36)	0.23
73	1272	4.2345(3)	3.48(2)	5.1206(4)	14.072(2)	319.562(38)	–0.22
73	1074	4.2304(4)	2.90(2)	5.1129(4)	14.070(2)	318.542(42)	–0.40
73	876	4.2217(5)	2.52(3)	5.1118(4)	14.069(2)	318.379(39)	0.02
73	673	4.2177(4)	1.91(2)	5.1231(4)	14.0643(8)	317.740(34)	0.08
73	294	4.2048(3)	0.93(2)	5.1015(4)	14.067(1)	317.066(43)	–0.30
100	673	4.1976(3)	4.25(2)	5.0961(4)	13.979(2)	314.406(40)	0.25
100	295	4.1860(5)	3.19(1)	5.0899(3)	13.980(2)	313.664(35)	–0.10
128	1278	4.2114(3)	6.73(2)	5.1026(5)	13.957(2)	314.703(50)	0.32
179	1273	4.1882(2)	9.84(2)	5.0773(3)	13.823(1)	308.599(39)	–0.12
179	1273	4.1882(2)	9.84(2)	5.0800(3)	13.826(2)	308.993(39)	0.11
179	1173	4.1883(3)	9.46(2)	5.0752(3)	13.837(3)	308.660(31)	–0.23
179	1073	4.1863(4)	8.88(2)	5.0744(3)	13.837(2)	308.567(31)	–0.20
179	973	4.1836(9)	8.62(5)	5.0732(3)	13.840(2)	308.472(31)	–0.11
179	873	4.1809(2)	8.34(6)	5.0727(3)	13.841(2)	308.453(32)	0.05
179	773	4.1816(4)	7.62(2)	5.0721(3)	13.841(2)	308.380(32)	–0.39
179	673	4.1746(6)	7.89(3)	5.0690(3)	13.846(2)	308.114(32)	0.05
179	573	4.1736(4)	7.37(2)	5.0704(3)	13.842(2)	308.183(33)	–0.09
179	473	4.1681(5)	7.45(3)	5.0688(3)	13.845(2)	308.047(33)	0.19
179	373	4.1644(5)	7.26(2)	5.0677(4)	13.845(2)	307.934(37)	0.21
179	300	4.1636(6)	6.89(3)	5.0720(4)	13.839(2)	308.325(29)	0.27
313	1273	4.1626(3)	13.23(2)	5.0501(4)	13.750(3)	303.680(78)	0.17
313	473	4.1347(2)	12.14(2)	5.0500(5)	13.650(3)	301.471(78)	0.49
313	300	4.1299(5)	11.93(3)	5.0293(5)	13.701(3)	300.117(53)	–0.27
446	1273	4.1448(5)	14.76(3)	5.0350(5)	13.650(3)	299.683(78)	0.04
446	1073	4.1379(6)	15.56(4)	5.0350(5)	13.620(3)	299.024(78)	0.23
446	873	4.1300(6)	15.47(4)	5.0302(5)	13.600(3)	297.993(78)	0.16
446	673	4.1280(6)	14.47(4)	5.0300(5)	13.600(3)	297.992(66)	–0.19

Note: Lattice parameters *a* and *c* for MgO and ilmenite given in angstroms, unit-cell volumes *V* given in cubic angstroms. Numbers in parentheses are 1σ error in last digit. Δ*P* denotes difference between measured *P* and *P* calculated for given *T* and ilmenite unit-cell volume *V* using the Birch-Murnaghan (BM) EOS parameters listed in Table 5.

unit-cell volume calculation.

At ambient conditions, the derived unit-cell volume of the synthetic sample is V_0 = 319.12 ± 0.26 Å^3. The best-fit 1 bar isothermal bulk modulus K_{T0} for this sample is 181 ± 7 GPa. The pressure derivative of the 1 bar isothermal bulk modulus K_0' can be refined to 3 ± 1. The temperature derivative of the 1 bar isothermal bulk modulus, dK/dT = –0.021 ± 0.007 GPa/K.

Because of the smaller number of data points obtained in this study, not all EOS parameters can be refined for the natural ilmenite sample. Its V_0 = 314.75 ± 0.23 (1σ) Å^3, is significantly smaller than that of the synthetic sample (see next section). With K_0' and dK/dT fixed to the best-fit values obtained for the synthetic sample, the 1 bar isothermal bulk modulus derived for the natural ilmenite sample is 165 ± 6 GPa.

DISCUSSION

Ilmenite at ambient conditions

Previous measurements of ilmenite unit-cell volumes at ambient conditions average 314.9 Å^3, with individual values ranging from 311.6 to 316.9 Å^3 (Table 1). The value measured for our natural terrestrial ilmenite, 314.75 ± 0.23 Å^3, coincides with the average literature value.

The unit-cell volumes of several lunar ilmenite grains have also been measured previously. Their unit-cell volumes with an average value of 315.4 Å^3 are slightly larger than the average of their terrestrial equivalents. Thorpe et al. (1977) attributed this volume difference to the fact that the *c* axis of lunar ilmenite is elongated (14.08 vs. 14.05 Å). The possible reason for this, first

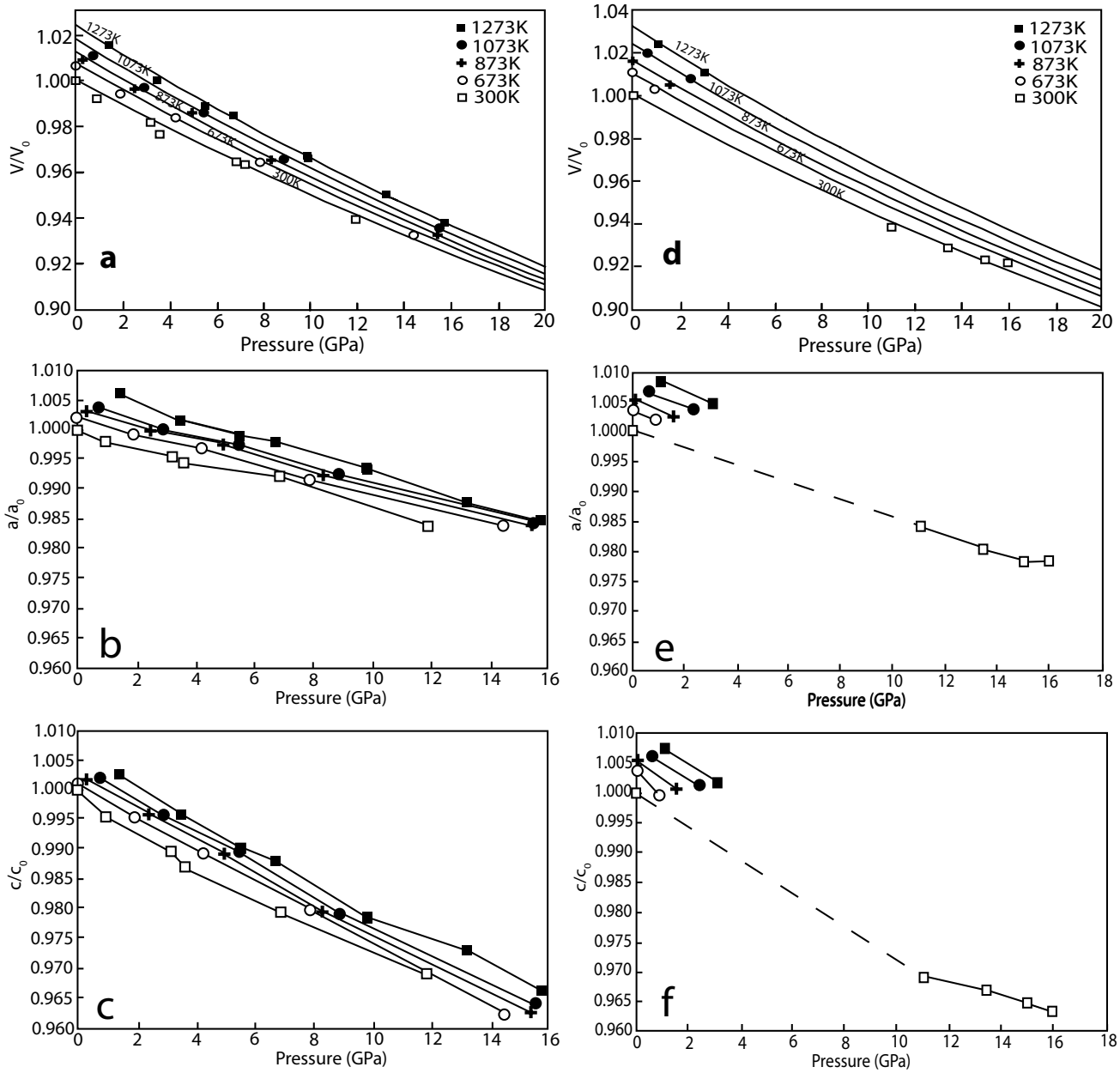

FIGURE 4. Behavior of the unit-cell dimensions of the synthetic ilmenite (**a**, **b**, and **c**) and the natural ilmenite (**d**, **e**, and **f**) at various pressures and temperatures. For clarity, only data obtained at 1273, 1073, 873, 673, and 300 K are shown. Curves in **a** and **d** are derived from the EOS parameters given in Table 5.

TABLE 5. Best-fit high-temperature Birch-Murnaghan equation of state parameters for our samples, compared to the results of Wechsler and Prewitt (1984)

EOS parameter	Synthetic ilmenite (this study)	Natural ilmenite (this study)	Synthetic ilmenite (Wechsler and Prewitt)
V_0 (Å^3)	319.12(26)	314.75(23)	315.84
K_{T0} (GPa)	181(7)	165(6)	177(3)
K_0'	3.0(10)	3.0*	4*
$\alpha_0 \times 10^5$ (K^{-1})	1.12(42)	1.62(45)	2.70(1)
$\alpha_1 \times 10^8$ (K^{-2})	1.63(57)	2.03(58)	0.34(1)
dK/dT (GPa/K)	−0.021(7)	−0.021*	−0.02*

Note: V_0 is the unit-cell volume at room conditions, K_{T0} is the isothermal bulk modulus, K_0' is its pressure derivative, α_0 is the first-order parameter of the thermal expansivity, α_1 is the second-order parameter (see Eq. 2). Numbers in parentheses are 1σ error in last digit.
* Denotes fixed value.

put forward by Bayer et al. (1972), is that the average ionic radius of Fe^{2+} and Ti^{4+} (~0.75 Å) exceeds that of Fe^{3+} (~0.69 Å). The absence of Fe^{3+} in the Moon should therefore lead to expansion of the ilmenite lattice in the *c* direction. We note that neither terrestrial nor lunar ilmenite consists of pure $FeTiO_3$. The effect of variations in minor element (Mg, Al, Cr) contents on unit-cell volume remains unknown.

Although previous studies have claimed to have synthesized Fe^{3+}-free $FeTiO_3$ ilmenite, the average reported unit-cell volume in those samples is 315.8 Å^3, significantly smaller than our value (V_0 = 319.12 ± 0.26 Å^3). Previous studies did not perform any analyses to constrain the iron oxidation state in their synthetic samples. The sample used by Wechsler and Prewitt (1984; V_0 = 315.84 Å^3) was synthesized using a stoichiometric mix of $Fe+Fe_2O_3+TiO_2$, loaded in an Ag capsule and reacted in a piston-cylinder press at 2 GPa and 1273 K for one day. In the absence of a true f_{O_2} buffer, it is possible that this procedure led to synthesis of Fe^{3+}-bearing ilmenite. Unfortunately, the starting composition of the Yamanaka et al. (2007) sample is not documented, so we cannot evaluate its purity or oxidation state. In addition, previous studies did not monitor and control the oxidation state of the sample during compression and heating experiments.

In contrast, our Mössbauer analyses discussed above demonstrate that the Fe^{3+} content of our synthetic sample was negligible, and that no oxidation occurred during the experiments. This provides a possible explanation for the larger observed unit-cell volume of our synthetic sample compared to previously reported values.

Ilmenite at high pressure and temperature

In Figure 4, the unit cells of our Fe^{3+}-free synthetic ilmenite and our Fe^{3+}-bearing natural ilmenite are compared. As mentioned above, only two prior studies of ilmenite behavior at high pressure or high temperature exist. Wechsler and Prewitt (1984) performed one set of experiments at room pressure with increasing temperature, and one at room temperature with increasing pressure. Yamanaka et al. (2007) also performed high pressure experiments at room temperature. Our results for both samples are compared with the results from these previous studies in Figure 5 and Table 5.

The significant difference in unit-cell volume at ambient conditions between our reduced ilmenite and the natural sample as well as the two other studies clearly persists to high pressures (Fig. 5a). The near-parallel evolution of the room-temperature

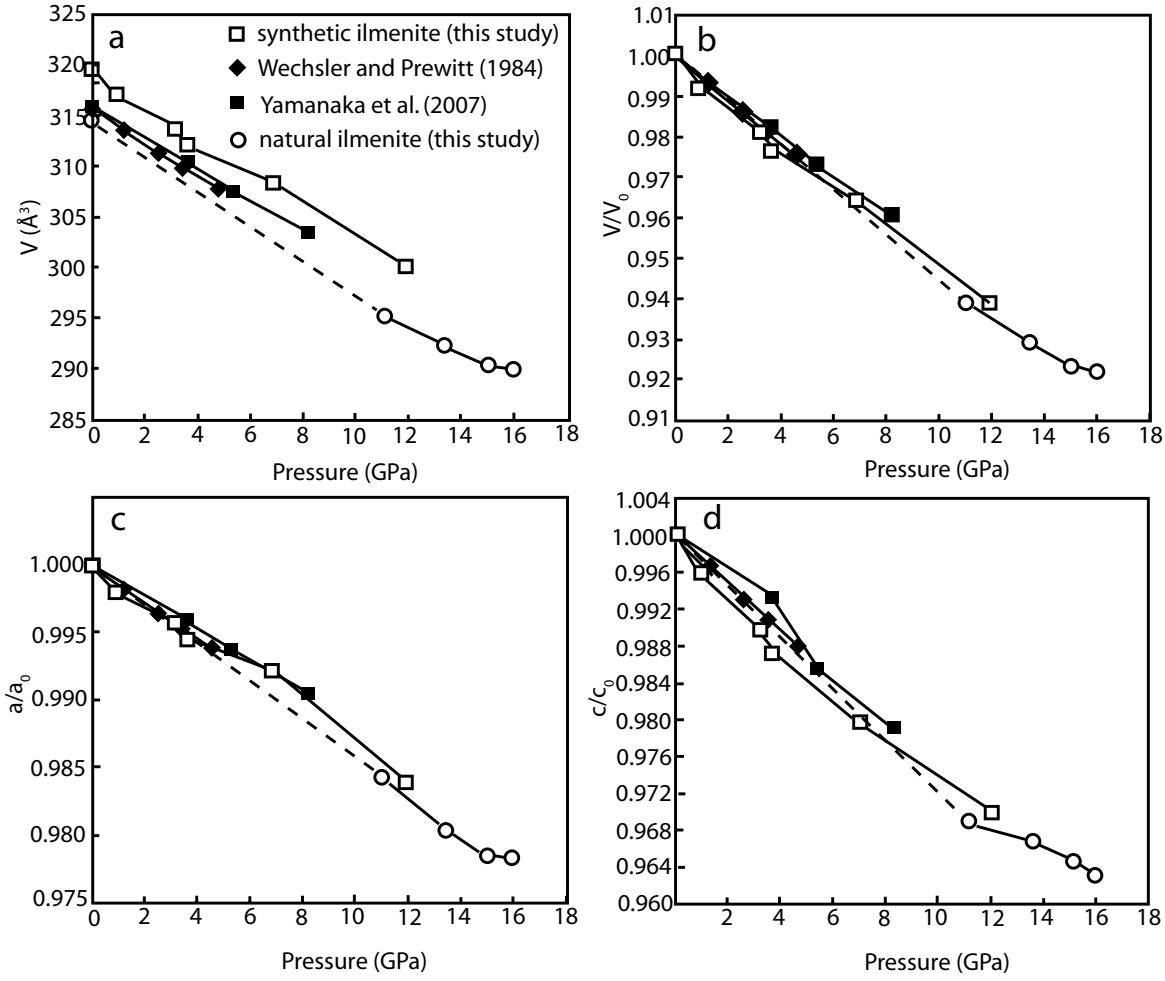

FIGURE 5. Room-temperature volume (**a**) and unit-cell dimensions (**b**, **c**, and **d**) as a function of pressure of reduced synthetic and oxidized natural ilmenite (this study) compared to literature values for samples of unknown oxidation state (Wechsler and Prewitt 1984; Yamanaka et al. 2007).

unit-cell volumes with pressure for all samples is reflected in the similar room-temperature bulk moduli K_{T0} of 181 ± 7 GPa (this study, synthetic), 177 ± 3 GPa (Wechsler and Prewitt 1984), and 165 ± 5 GPa (this study, natural) coupled with a pressure derivative of 3 ± 1 in all cases. The refined temperature derivative of the bulk modulus, $dK/dT = -0.021 \pm 0.007$, is also within the error of the value used by Wechsler and Prewitt (1984). In summary, although their unit-cell volumes exhibit significant variations, other thermal EOS parameters are similar for reduced and oxidized ilmenites.

Figures 5c and 5d show that in detail, minor compressibility differences are caused primarily by small differences in *c* axis behavior. We conclude that the *c* axis of low-Fe^{3+} ilmenite is longer and perhaps slightly more compressible than the *c* axis of oxidized, high-Fe^{3+} ilmenite.

The unit-cell volume of the synthetic ilmenite from Wechsler and Prewitt (1984) at ambient condition is 315.8 Å^3 before heating and 316.1 Å^3 after heating, which is very close to the volume of lunar ilmenites (V_0 = 315.4 Å^3). Our reduced synthetic ilmenite unit cell (V_0 = 319.1 Å^3) is larger than that of the natural lunar ilmenites. As noted above, lunar ilmenites can contain significant amounts of minor elements, including Mg, Cr, and Al. In particular, the MgO content varies from 0 to 8 wt% in lunar ilmenite. Adding Mg to $FeTiO_3$ ilmenite results in changes in both the volume and mass of its unit cell: Liebermann (1976) studied end-member $MgTiO_3$ (geikilite) at room conditions and measured a unit-cell volume of 307.44 Å^3. Wechsler and von Dreele (1989) measured V_0 of $MgTiO_3$ to be 307.48 Å^3. This is much smaller than the volume of pure $FeTiO_3$, providing a plausible explanation for the smaller unit-cell volume of lunar ilmenites than our value. However, lunar ilmenite 10047 (Table 1) is close in composition to the pure $FeTiO_3$ end-member. Its unit-cell volume at room conditions was determined by Bayer et al. (1972) to be V_0 = 315.8 Å^3. This is still 1.1% smaller than our measurement for synthetic reduced $FeTiO_3$, and we do not have a satisfactory explanation for this discrepancy.

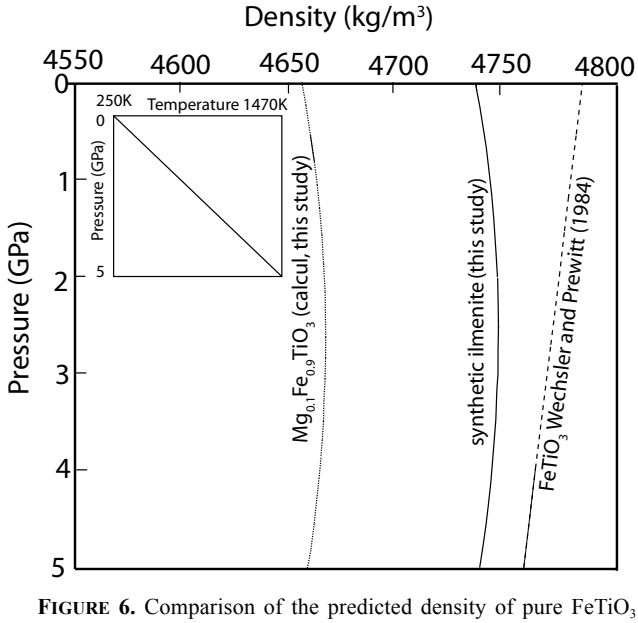

FIGURE 6. Comparison of the predicted density of pure $FeTiO_3$ ilmenite in the interior of the Moon, using our thermal EOS data (solid black line) and previous EOS estimates Wechsler and Prewitt (1984; dotted line). The effect of replacing 10 mol% of Fe with Mg is also shown (dashed line). For the $Fe_{0.9}Mg_{0.1}TiO_3$ profile, we calculated a V_0 of 180 GPa and a unit-cell volume of 317.96 Å^3 based on the study on geikielite $MgTiO_3$ by Liebermann (1976) (V_0 = 307.44 Å^3 and a room-temperature bulk modulus of 169 GPa). A simplified linear lunar temperature profile (T = 250 K at P = 0 GPa, T = 1470 K at P = 5 GPa) is assumed.

CONCLUDING REMARKS

We determined the thermal equation of state of $FeTiO_3$ containing virtually no Fe^{3+}, and have shown that its unit-cell volume is about 1.5% larger than those of terrestrial ilmenite. Other thermal EOS parameters differ only slightly. Our results provide more appropriate input parameters for thermo-chemical models of lunar interior evolution, in which reduced ilmenite plays a critical role. Figure 6 shows a predicted density profile for ilmenite in the lunar interior using our data obtained with the reduced synthetic ilmenite, compared to values obtained using the Wechsler and Prewitt (1984) EOS parameters. The differences in EOS parameters are reflected in a ~1% shift in the position of the profile, as well as a subtle change in the shape of the profile. Figure 6 also illustrates that replacing 10 mol% of Fe in $FeTiO_3$ by Mg leads to a ~2% reduction in ilmenite density (assuming a linear relation of V_0 and bulk modulus with composition between the two end-members $FeTiO_3$ and $MgTiO_3$). The effect of using our new thermal EOS on lunar ilmenite density is therefore equivalent to the effect of increasing the Mg content of lunar interior ilmenite by ~5 mol%.

ACKNOWLEDGMENTS

We thank De Beers Group Services for supplying the natural ilmenite sample, Wim Lustenhouwer for support during electron microprobe analysis, and Xinyang Chen and Zeyu Li for support during synchrotron experiments. We thank Jelle van Sijl for creating a GSAS conversion program for this work. Comments by three anonymous reviewers significantly improved the quality of this manuscript. Portions of this work were performed at GeoSoilEnviroCARS (Sector 13), Advanced Photon Source (APS), Argonne National Laboratory. GeoSoilEnviroCARS is supported by the National Science Foundation-Earth Sciences (EAR-0217473), Department of Energy-Geosciences (DE-FG02-94ER14466), and the State of Illinois. Use of the APS was supported by the U.S. Department of Energy, Office of Science, Office of Basic Energy Sciences, under contract no. W-31-109-ENG-38, partially by COMPRES, the COnsortium for Materials Properties Research in Earth Sciences under NSF Cooperative Agreement EAR06-49658. J.L. acknowledges support by NASA grant NNX09AB946 and NSF grants EAR069639 and EAR0738973. B.C. acknowledges support by the Texaco Postdoctoral Fellowship from the Division of Geological and Planetary Sciences, California Institute of Technology. This work was funded by a European Science Foundation EURYI award to W.v.W.

REFERENCES CITED

Angel, R.J. (2000) Equations of state. In R.M. Hazen and R.T. Downs, Eds., High-Temperature and High-Pressure Crystal Chemistry, 41, p. 35–59. Reviews in Mineralogy and Geochemistry, Mineralogical Society of America, Chantilly, Virginia.

Barth, T.F.W. and Posnjak, E. (1934) The crystal structure of Ilmenite. Zeitschrift für Kristallographie, 88, 265–270.

Bayer, G., Felsche, J., and Schulz, H. (1972) X-ray study and Mössbauer spectroscopy on lunar ilmenites (Apollo 11). Earth and Planetary Science Letters, 16, 273–274.

de Vries, J., van den Berg, A., and van Westrenen, W. (2010) Formation and evolution of a lunar core from ilmenite-rich magma ocean cumulates. Earth and Planetary Science Letters, 292, 139–147.

Hess, P.C. and Parmentier, E.M. (1995) A model for the thermal and chemical evolution of the Moon's interior: Implications for the onset of mare volcanism. Earth and Planetary Science Letters, 134, 501–514.

Klemme, S., Günther, D., Hametner, K., Prowatke, S., and Zack, T. (2006) The partitioning of trace elements between ilmenite, ulvospinel, armalcolite and silicate melts with implications for the early differentiation of the moon. Chemical Geology, 234, 251–263.

Larson, A.C. and von Dreele, R.B. (2004) General structure analysis system (GSAS). Los Alamos National Laboratory Report LAUR 86-748.

Leinenweber, K., Mosenfelder, J., Diedrich, T., Soignard, E., Sharp, T.G., Tyburczy, J.A., and Wang, Y. (2006) High-pressure cells for in-situ multi-anvil experiments. High Pressure Research, 26, 283–292.

Liebermann, R.C. (1976) Elasticity of ilmenites. Physics of the Earth and Planetary Interiors, 12, 5–10.

Liu, L. (1975) High-pressure phase transformations and compressions of ilmenite and rutile: I. Experimental results. Physics of the Earth and Planetary Interiors, 10, 167–176.

Lucey, P.G., Taylor, G.J., and Malaret, E. (2006) Abundance and distribution of iron on the Moon. Science, 268, 1150–1153.

Ming, L.C., Kim, Y.-H., Uchida, T., Wang, Y., and Rivers, M. (2006) In situ X-ray diffraction study of phase transitions of $FeTiO_3$ at high pressures and temperatures using a large-volume press and synchrotron radiation. American Mineralogist, 91, 120–126.

Pavicevic, M., Ramdohr, P., and El Goresy, A. (1972) Electron microprobe investigations of the oxidation states of Fe and Ti in ilmenite in Apollo 11, Apollo 12, and Apollo 14 crystalline rocks. Proceedings of the Third Lunar Science Conference, Supplement 3, Geochimica et Cosmochimica Acta, 1, 295–303.

Raymond, K.N. and Wenk, H.R. (1971) Lunar ilmenite (refinement of the crystal structure). Contributions to Mineralogy and Petrology, 30, 135–140.

Shearer, C.K., Hess, P.C., Wieczorek, M.A., Pritchard, M.E., Parmentier, E.M., Borg, L.E., Longhi, J., Elkins-Tanton, L.T., Neal, C.R., Antonenko, I., Canup, R.M., Halliday, A.N., Grove, T.L., Hager, B.H., Lee, D.-C., and Wiechert, U. (2006) Thermal and magmatic evolution of the Moon. In B.L. Jolliff, M.A. Wieczorek, C.K. Shearer, and C.R. Neal, Eds., New Views of the Moon, 60, p. 365–518. Reviews in Mineralogy and Geochemistry, Mineralogical Society of America, Chantilly, Virginia.

Shirane, G., Cox, D.E., Takei, W.J., and Ruby, S.L. (1962) A study of the magnetic properties of the $FeTiO_3$-Fe_2O_3 system by neutron diffraction and the Mössbauer effect. Journal of the Geophysical Society of Japan, 17, 1598–1611.

Snyder, G.A., Taylor, L.A., and Neal, C.R. (1992) A chemical model for generating the sources of mare basalts: combined equilibrium and fractional crystallization of the lunar magmasphere. Geochimica et Cosmochimica Acta, 56, 3809–3823.

Speziale, S., Zha, C.-S., Duffy, T.S., Hemley, R.J., and Mao, H.-k. (2001) Quasi-hydrostatic compression of magnesium oxide to 52 GPa: Implications for the pressure-volume-temperature equation of state. Journal of Geophysical Research, 106, 515–528.

Syono, Y., Takei, G., and Ito, A. (1981) Single crystal X-ray and Mössbauer study of shocked ilmenite to 80 GPa. Physics and Chemistry of Minerals, 7, 82–87.

Tange, Y., Nishihara, Y., and Tsuchiya, T. (2009) Unified analyses for P-V-T equation of state of MgO: a solution for pressure-scale problems in high P-T experiments. Journal of Geophysical Research, 114, B03208.

Taylor, S.R. (1982) Planetary science: A Lunar Perspective, p. 481. Lunar and Planetary Institute, Houston.

Thorpe, A.N., Minkin, J.A., Senftle, F.E., Alexander, C., Briggs, C., Evans, Jr., H.T., and Nord, Jr., G.L. (1977) Cell dimensions and antiferromagnetism of lunar and terrestrial ilmenite single crystals. Journal of the Physics and Chemistry of Solids, 38, 115–123.

Toby, B.H. (2001) EXPGUI, a graphical user interface for GSAS. Journal of Applied Crystallography, 34, 210–213.

van Westrenen, W., Van Orman, J.A., Watson, H., Fei, Y., and Watson, E.B. (2003) Assessment of temperature gradients in multianvil assemblies using spinel layer growth kinetics. Geochemistry, Geophysics, Geosystems, 4, 1036, doi:10.1029/2002GC000474.

van Westrenen, W., Li, J., Fei, Y., Frank, M.R., Hellwig, H., Komabayashi, T., Mibe, K., Minarik, W.G., Van Orman, J.A., Watson, H.C., Funakoshi, K.-I., and Schmidt, M.W. (2005) Thermoelastic properties of $(Mg_{0.64}Fe_{0.36})O$ ferropericlase based on in situ X-ray diffraction to 26.7 GPa and 2173 K. Physics of the Earth and Planetary Interiors, 151, 163–176.

Virgo, D., Luth, R.W., Moats, M.A., and Ulmer, G.C. (1988) Constraints on the oxidation state of the mantle: an electrochemical and ^{57}Fe Mössbauer study of mantle-derived ilmenites. Geochimica et Cosmochimica Acta, 52, 1781–1794.

Wang, Y., Rivers, M., Sutton, S., Nishiyama, N., Uchida, T., and Sanehira, T. (2009) The large-volume high-pressure facility at GSECARS: A "Swiss-army-knife" approach to synchrotron-based experimental studies. Physics of the Earth and Planetary Interiors, 174, 270–281.

Wechsler, B.A. and Prewitt, C.T. (1984) Crystal structure of ilmenite ($FeTiO_3$) at high temperature and at high pressure. American Mineralogist, 69, 176–185.

Wechsler, B.A. and von Dreele, R.B. (1989) Structure refinements of Mg_2TiO_4, $MgTiO_3$, and $MgTi_2O_5$ by time-of-flight neutron powder diffraction. Acta Crystallographica, B45, 542–549.

Wu, X., Steinle-Neumann, G., Narygina, O., Kantor, I., McCammon, C., Pascarelli, S., Aquilanti, G., Prakapenka, V., and Dubrovinsky, L. (2009) Iron oxidation state of $FeTiO_3$ under high pressure. Physical Review B, 79, 094106.

Wyatt, B.A., Baumgartner, M., Anckar, E., and Grutter, H. (2004) Compositional classification of kimberlitic and non-kimberlitic ilmenite. Lithos, 77, 819–840.

Yamanaka, T., Komatsu, Y., and Nomori, H. (2007) Electron density distribution of $FeTiO_3$ ilmenite under high pressure analysed by MEM using single crystal diffraction intensities. Physics and Chemistry of Minerals, 34, 307–318.

Manuscript received September 29, 2009
Manuscript accepted July 3, 2010
Manuscript handled by Artem Oganov